Why are some solar wind pressure pulses followed by geomagnetic storms?

Alexandra Ruth Fogg[1]

C. M. Jackman[1], **I. Coco**[2], **L. Douglas Rooney**[3], **D. M. Weigt**[1], **M. Lester**[4]

[1]School of Cosmic Physics, DIAS Dunsink Observatory, Dublin Institute for Advanced Studies, Dublin 15, Ireland
[2]Istituto Nazionale di Geofisica e Vulcanologia, Rome, Italy
[3]Trinity College Dublin, Dublin, Ireland
[4]School of Physics and Astronomy, University of Leicester, United Kingdom

Key Points:

- There is a solar cycle dependence to the occurrence and magnitude of sudden commencements (SCs)
- Sudden storm commencements (SSCs) are driven by higher magnitude and/or shorter duration pressure pulses
- The magnetosphere is primed by stronger solar wind / interplanetary magnetic field and higher geomagnetic activity for SSCs

Corresponding author: Alexandra Ruth Fogg, `arfogg@cp.dias.ie`

Abstract

Rapid increases in solar wind dynamic pressure, known as solar wind pressure pulses, compress the Earth's magnetosphere and can rapidly restructure the electrodynamics within. The propagation of pressure pulse effects into the magnetosphere is known as a geomagnetic sudden commencement (SC). SCs can be further subdivided into compressions which are rapidly followed by a geomagnetic storm (a sudden storm commencement, SSC) and those which are not (a sudden impulse, SI). In this paper, SSCs and SIs are compared and contrasted, and we examine in particular the differences between the pressure pulses that drive SSCs/SIs, and explore the physical conditions of the magnetosphere before pressure pulse arrival. Firstly, it is shown that SSCs are more likely to be driven by pressure pulses with higher magnitude and/or shorter rise time. Secondly, the magnetosphere is primed by stronger driving conditions and higher geomagnetic activity prior to SSCs than SIs. Finally, there is a solar cycle dependence in the occurrence and magnitude of solar wind pressure pulses.

Plain Language Summary

The solar wind's dynamic pressure controls the size of the cavity the Earth's magnetic field forms in space. When the pressure increases rapidly, this is known as a solar wind pressure pulse. Pressure pulses can affect currents and magnetic fields within the Earth's space environment, and can have serious space weather implications. In this paper, the differences between pressure pulses that are followed by geomagnetic storms (large releases of energy in the Earth's system), and those that are not are investigated. The state of the Earth's system before the arrival of the pressure pulse is also considered, and its contribution to the resulting space weather effects. It is shown that larger pressure pulses are more likely to trigger a geomagnetic storm. Additionally, analysis presented shows that the Earth's system may already be active prior to the triggering of these storms. Finally, the occurrence and strength of pressure pulse events follows solar activity.

1 Introduction

The size and shape of the Earth's magnetosphere is controlled by the balance of solar wind dynamic pressure and magnetic pressure from Earth's magnetic field. The solar wind dynamic pressure has been observed to vary over short and long timescales. When it increases rapidly over timescales of minutes, this is known as a solar wind pressure pulse. When a pressure pulse impacts the magnetosphere and its effects are propagated within the terrestrial space environment, this is known as a geomagnetic sudden commencement (SC, Araki, 1994; Fujita, 2019), and coined a 'Geospace Concussion' by Shi et al. (2022). SCs are often identified by a rapid increase in the ring current index SYM-H (e.g., Hori et al., 2015), denoting an increase in the H component of the Earth's magnetic field in the equatorial plane (SYM-H is described in detail in section 2). Although not defined consistently in the literature, in this paper a sudden storm commencement (SSC, Taylor et al., 1994; Taylor, 1994; Kokubun, 1983; Burch, 1972) is defined as an SC which rapidly triggers a geomagnetic storm, otherwise, it is defined as a sudden impulse (SI, e.g., Takeuchi, Russell, & Araki, 2002).

Coronal mass ejections (CMEs) and corotating interaction regions (CIRs) are the cause of most of the solar wind pressure pulses which drive SCs (e.g., Zuo et al., 2015). In fact, Veenadhari et al. (2012) showed that SCs are driven by CMEs with twice the average CME speed, and that SC amplitude increases with increasing shock speed or Mach number. Taylor et al. (1994) determined that SSCs are driven by the violent eruptions of plasma from the solar corona which form CMEs. Conversely, Storm Gradual Commencements (SGCs, storms that do not follow a rapid compression or SC) were shown to be driven by CIR compressions (Taylor et al., 1994). When there is no subsequent storm within 6-12 hours (Taylor et al., 1994), a positive SI (+SI) may be generated from a rapid

increase in pressure, and a negative SI (-SI) may be generated from a rapid decrease in pressure. It is important to note that this criterion is imperfect: for some magnetic clouds the storm that follows can start beyond 12 hours later (e.g., Gopalswamy, 2008), although the average and median delay times shown by Gopalswamy (2008) are below 12 hours. There is a solar cycle dependence to the occurrence of many solar phenomena, for example the occurrence rate of CMEs peaks around solar cycle maximum and during the declining phase of the solar cycle the Sun's tilted dipole leads to a regular pattern of CIR compressions (Jackman et al., 2004, and references therein) and rarefactions during each solar rotation (Gosling, 1996; Crooker et al., 1999). Therefore a solar cycle dependence of SCs is anticipated, and indeed a solar cycle dependence to the occurrence of SCs was presented by Fogg (2021), and a 10-11 year periodicity in SSCs was presented by Mendoza et al. (2003).

SCs and the pressure pulses that drive them have been detected by various authors with different methods and criteria. Coco et al. (2011) defined a pressure pulse as a change of at least 3 nPa in under 10 minutes, and detected about 300 events from roughly 4 years of ACE data. Recently, A. Boudouridis and Zesta (2021) used non-linear least squares fitting of a step-like function to detect pressure pulses from Wind and ACE data. SCs can be directly detected in the H component of ground magnetometer data (e.g., Araki et al., 2004), or equivalently in SYM-H: Hori et al. (2015) defined an SC signature as an increase of at least 5 nT with a minimum gradient of about 15 nT per 10 seconds.

Araki et al. (2004) investigated the relationship between the amplitude (dH) and the rise time (dT) of an SC using 108 events detected in low latitude ground magnetometer data. While they defined a relationship between dH and dT, they also defined these parameters in terms of controlling factors. Araki et al. (2004) notes that dT is controlled by the geoeffective magnetospheric length, solar wind velocity, characteristic Alfvén wave velocity and Mach number. The geoeffective magnetospheric length here is the distance between the subsolar point and the point tailwards beyond which compression effects do not propagate to the ground. Therefore they argue that a shock with a higher Mach number has a larger pressure increase, and sweeps over the entire magnetosphere quicker - this may produce an SC with a shorter dT and larger dH. Siscoe et al. (1968) showed that the amplitude of the SC is proportional to the amplitude of the pressure pulse; this relationship was later investigated by Russell et al. (1992); Takeuchi, Araki, et al. (2002) who both found that for each 1 $nPa^{\frac{1}{2}}$ in the square root of dynamic pressure, a change of 15.0-16.5 nT in the H component of ground magnetometers (and indeed SYM-H (Takeuchi, Araki, et al., 2002)) was observed.

Araki (1994) proposed a model for the propagation of SC effects into the terrestrial magnetosphere, via compressional mode propagation in the equatorial plane, and down field lines as Alfvén waves at high latitudes. The magnetosphere is compressed by the arrival of a pressure pulse, increasing the magnetopause current. The magnetopause current connects with a current along the compressional wavefront, which travels antisunwards through the equatorial plane. Within this current loop, the increased current results in an induced increase in the magnetic field: this is observed as an increase in the H component of magnetometer stations. SYM-H, the ring current index (Iyemori, 1990), is averaged over the H component of near-equatorial magnetometers, and hence observes this step change in magnitude.

The compressional wave couples to magnetic field lines to generate Alfvén waves which travel down to the high latitude ionosphere (this has been shown by Chi et al. (2006) to follow the Tamao (1964) path). Magnetometers observe a superposition of both the compressional and Alfvén mode waves: signatures of a step change for the former, and a bipolar oscillation for the latter. A larger component of compressional signature is observed at lower latitudes, and the signature is dominated by Alfvén component at higher latitudes (Fogg et al., 2023; Piersanti & Villante, 2016); there is also a local time dependence to the polarity of the Alfvén signature (Takeuchi, Araki, et al., 2002). Araki (1994)

suggests that the Alfvén and compressional components are observed simultaneously in magnetometer data, although Araki et al. (1997); Fujita et al. (2003) suggests that the Alfvén propagation follow the compressional mode. However, Fogg et al. (2023) presented some evidence that the Alfvén propagation reaches the high latitude ionosphere slightly before compressional components are seen at equatorial magnetometer stations.

SCs don't occur in isolation: as with any space weather phenomenon they can excite and restructure the electrodynamics within the magnetosphere. As a result of Alfvén propagation, Araki (1994) predicts a pair of high latitude convection vortices (now known as lobe reconnection cells) - tightly wound circulation of F region plasma - collocated with high latitude field aligned currents (FACs). These 'lobe' reconnection-type signatures (Crooker, 1992; Chisham et al., 2004; Imber et al., 2006) were observed around SI onset by Coco et al. (2008), and observed collocated with consistent FAC and auroral signatures by Fogg et al. (2023). Finally, Araki (1994) predicted that these signatures would be quickly countered by an opposing set of vortices and FACs, although more recent observations (e.g., Gillies et al., 2012) suggest that SC effects continue until the compression ends. Additionally, SCs have been shown to affect the electron density structure in the ionosphere (Coco et al., 2005, 2011; Gillies et al., 2012), enhance and/or alter twin cell ionospheric convection (Gillies et al., 2012; Hori et al., 2015), generate FACs (Fujita et al., 2003; Ozturk et al., 2017) and affect the size and intensity of the auroral oval (A. E. Boudouridis et al., 2003). Finally, Smith et al. (2021) related SC effects to geomagnetically induced currents, by presenting large rates of change in the H component of 12 magnetometer stations.

Although the effects of SIs and SSCs (and their umbrella term SCs) have been investigated, it is not clear why some SCs result in geomagnetic storms, and others do not. Hence, the fundamental question remains: why are some pressure pulses followed by geomagnetic storms and others are not? This is the premise for this study, a comparison of the solar wind drivers and preceding geomagnetic states for the two different types of SC. This will help to unravel how solar wind pressure pulses couple to the magnetosphere - ionosphere system, and how much the priming of the magnetosphere contributes to this coupling. Understanding which solar wind pressure pulses result in geomagnetic storms is of prime importance in space weather forecasting since geomagnetic storms are one of the key phenomena which influence space weather.

Firstly, the data used to probe the state of solar wind - magnetosphere - ionosphere coupling in this paper are described in section 2. Next, the SC event list used in the paper is described in detail in section 3, along with an examination of the events themselves and their relationship with solar cycle. Then statistical differences between SIs and SSCs are examined in terms of the events themselves, and the priming of the magnetosphere in section 4. Finally, a superposed epoch analysis of various solar wind and geomagnetic parameters is presented for SIs and SSCs in section 5, followed by concluding remarks.

2 Data

In this study, interplanetary magnetic field (IMF) and solar wind data, along with geomagnetic indices are used to characterise the effects of solar wind pressure pulses on the magnetosphere. All of these data are retrieved from the OMNI (Weimer et al., 2002, 2003; Weimer & King, 2008; King & Papitashvili, 2005) 1-minute resolution dataset, downloaded from OMNIWeb: `https://omniweb.gsfc.nasa.gov/hw.html`. Firstly, components $B_{Z,GSM}$, $B_{Y,GSM}$ and total magnetic field magnitude $B_T = \sqrt{B_X^2 + B_Y^2 + B_Z^2}$ are used to characterise the coupling of the IMF to the Earth's magnetosphere. To represent solar wind - magnetosphere coupling, the solar wind flow speed (V_{SW}), particle density (N_{SW}) and dynamic pressure (P_{SW}) are also retrieved.

Provided by the World Data Center for Geomagnetism, Kyoto, the auroral electrojet (AE, World Data Center for Geomagnetism Kyoto et al., 2015; Davis & Sugiura, 1966) and ring current (SYM-H, Iyemori, 1990) indices, as well as the polar cap index (PC_N, provided by the World Data Center for Geomagnetism, Copenhagen, Stauning (2013); Troshichev et al. (1979); Troshichev and Andrezen (1985)) are used to characterise geomagnetic activity. The polar cap index (PC_N) is proportional to the variation in the trace of a polar latitude magnetometer, and incorporates information on the solar wind and IMF variability. The auroral electrojet index (AE) and ring current index (SYM-H) are derived from the H component of magnetometers at auroral (AE), and equatorial (SYM-H) latitudes, and which change as a result of variations in the local magnetic field as a result of overhead currents. All are available as part of the OMNI data set and are retrieved from OMNIWeb. PC_N is an indicator of the speed of flux transport across the polar cap, and equivalently the strength of polar ionospheric currents and convection. AE is an indicator of the strength of auroral electrodynamics, and famously shows excitations relating to substorm dynamics. SYM-H provides an estimate of the strength of the equatorial ring current, and is most often used as an indicator of geomagnetic storm activity; however it also shows rapid positive excursions as a result of pressure pulse arrival (e.g., Hori et al., 2015).

Finally, the sunspot number is used to characterise solar activity. Both the monthly sunspot number and the 13 month smoothed sunspot number are used to characterise the stage of the solar cycle; these are both obtained from Sunspot Index and Long-term Solar Observations (SILSO) at the Royal Observatory of Belgium (2020).

3 Sudden Commencement Events and Exploration of Parameter Space

To allow a statistical study of SC events, the catalogue of SC events compiled by the Observatori de l'Ebre (hereafter called OE events, Observatori de l'Ebre, 2020) was used, including all positive events (increases) from 1995 to 2017 inclusive (a total of 410 events). OE events are freely available from: `https://www.obsebre.es/en/rapid`. At date of download, definitive OE events are available until 2019. However, auroral indices in the OMNI dataset (described in section 2) are available until part way through 2018. Since complete datasets from both sources are needed, in this study the interval of overlap ends in 2017. The window from 1995 was used as this gives a broad parameter space of two solar cycles, and is a time period over which OMNI data are continuously available. The OE search algorithm looks for sudden increases in the magnetic field in magnetometer data at roughly equatorial stations (up to $\approx 33^\circ$N), and classifies an SC as an increase with gradient of at least 3 nT minute^{-1}. For the OE dataset, entries from 2006 (at time of writing), include a definition of whether an event is an SI/SSC. If, within the next 48 hours either Dst (roughly equivalent to SYM-H) decreases to at least -50 nT or the Kp (a measure of the disturbance in the geomagnetic field) index rises to at least 5, they define the event as an SSC, otherwise, it is flagged as an SI. In this study, the OE definition seperating SSCs and SIs is considered too conservative, and a different definition is utilised, and described below.

SC events have been automatically detected by authors using various different criteria, sometimes within SYM-H or H component data, and other times in the solar wind pressure data, as described in section 1. However, the OE event list was chosen for this study as it provides a multi-decadal archive, and is freely and openly available online, which enhances the repeatability and openness of this research.

The distributions of characteristics of SC events is presented in Figure 1. In Figure 1(a), the distribution of SC amplitude, the magnitude of the increase in nT, is presented. The median of the distribution is 19.04 nT, and the distribution extends into some extreme events with magnitude greater than 120 nT. Figure 1(b) contains the distribution of the event duration or 'rise time', the minutes spent increasing by the recorded

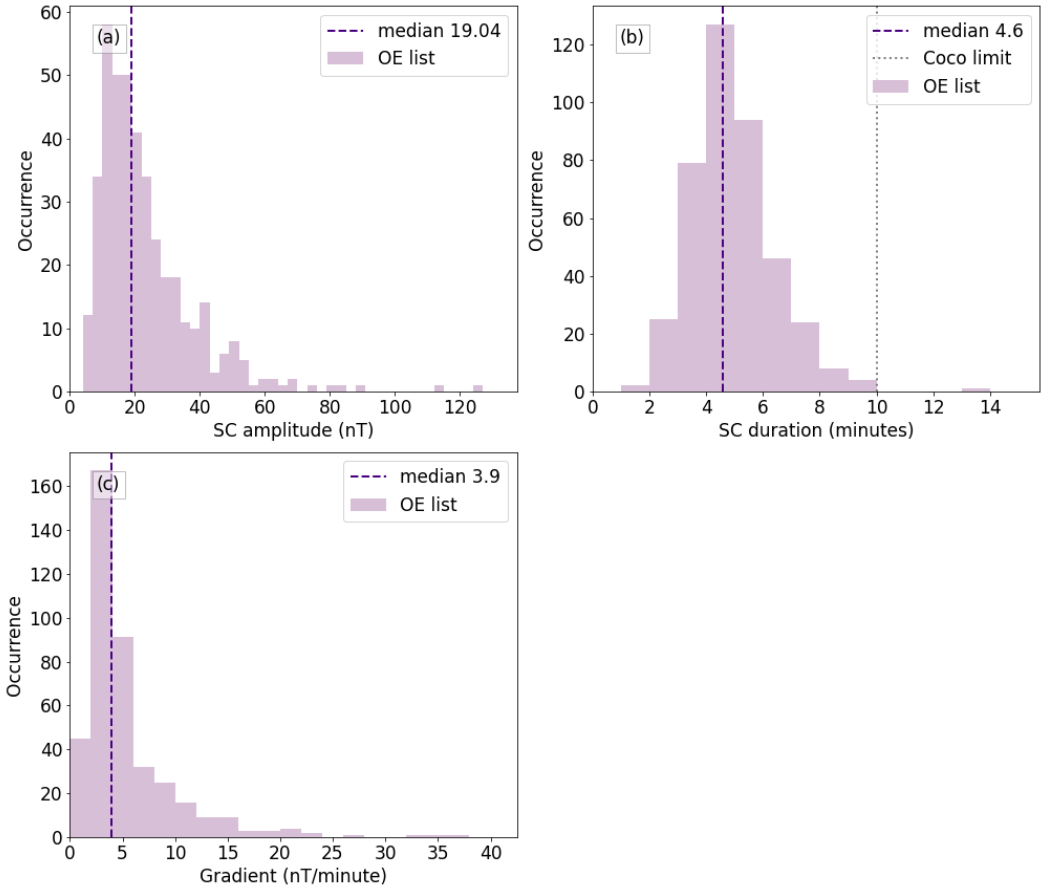

Figure 1. Histograms of SC (a) event amplitude (b) event duration or 'rise time' (c) event rise gradient from the OE event list (410 events total). Dashed purple line indicates the median of the distribution. In panel (b) the dotted grey line indicates the 10 minute limit of Coco et al. (2011).

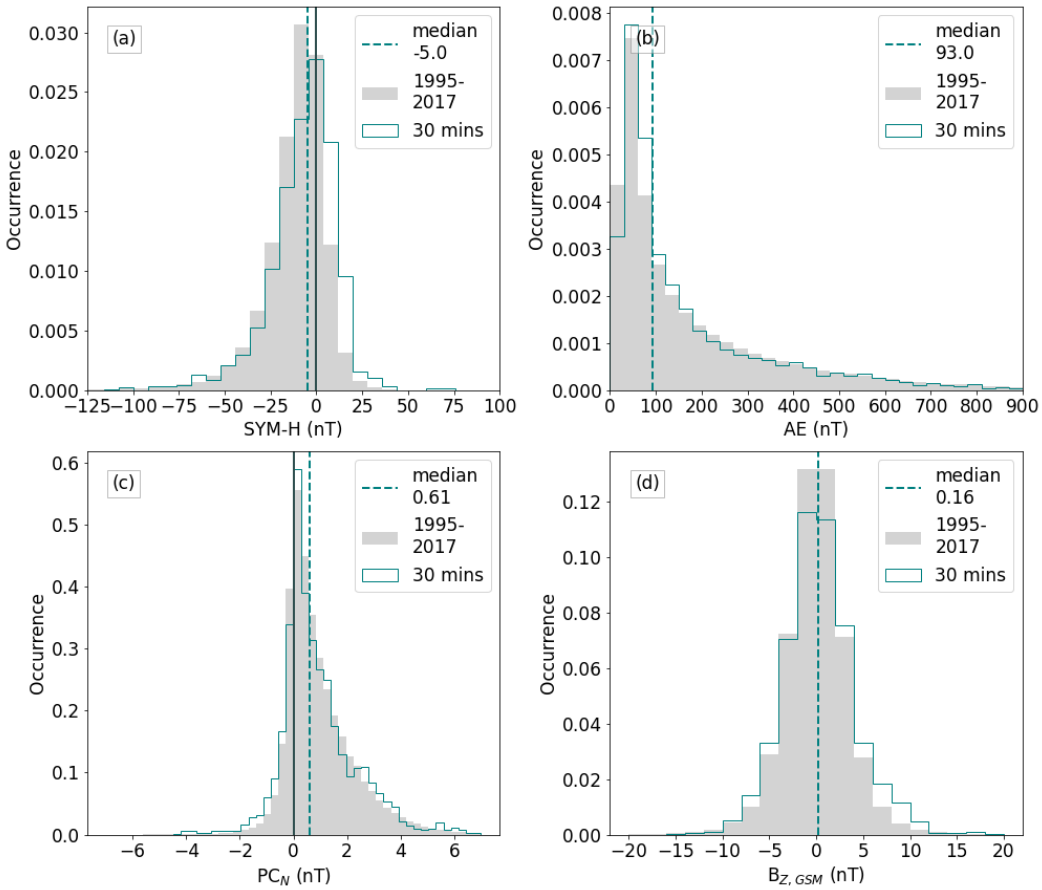

Figure 2. Normalised histograms (counts divided by total number of counts and bin width) of (a) SYM-H (b) AE (c) PC_N (d) $B_{Z,GSM}$. Filled grey histogram is data from the full period 1995-2017 inclusive, teal line histogram is data from the 30 minutes preceding each OE SC event. The median of the teal distribution is indicated with a dashed vertical line. Where appropriate, zero is indicated with a solid black vertical line.

amplitude, which has a median of 4.6 minutes. The distribution is mostly symmetrical, with few events above the 10 minute rise time limit of Coco et al. (2011) (indicated on the panel with a dotted grey line). Finally, the distribution of the gradient, the amplitude divided by the duration, is presented in Figure 1(c). The median value is 3.9 nT minute^{-1}, and the distribution follows a similar shape to that for the amplitude.

To ensure the parameter space for the OE SC events is not biasing results, the distribution of different geomagnetic indices and IMF B_Z are compared for the full period 1995-2017, and just in the 30 minutes preceding each SC (the sample is a concatenated list of the parameter from 30 minutes before each SC onset). The parameters within this 30 minute window will describe how the magnetosphere is primed preceding the SC; a 30 minute window was used as beyond this the driving conditions may vary further, including driving by events other than pressure pulses. In Figure 2(a), the distribution of SYM-H for 1995-2017 inclusive is plotted as a grey shade, and for the 30 minute window as a teal line histogram. The two distributions are very similar, and the median value for the 30 minute window is -5 nT. The distributions for AE (Figure 2(b)), PC_N (Figure 2(c)) and IMF B_Z (Figure 2(d)) are also similar for both 1995-2017 and the 30 minute window. This quantitative examination of baseline conditions shows that on average the

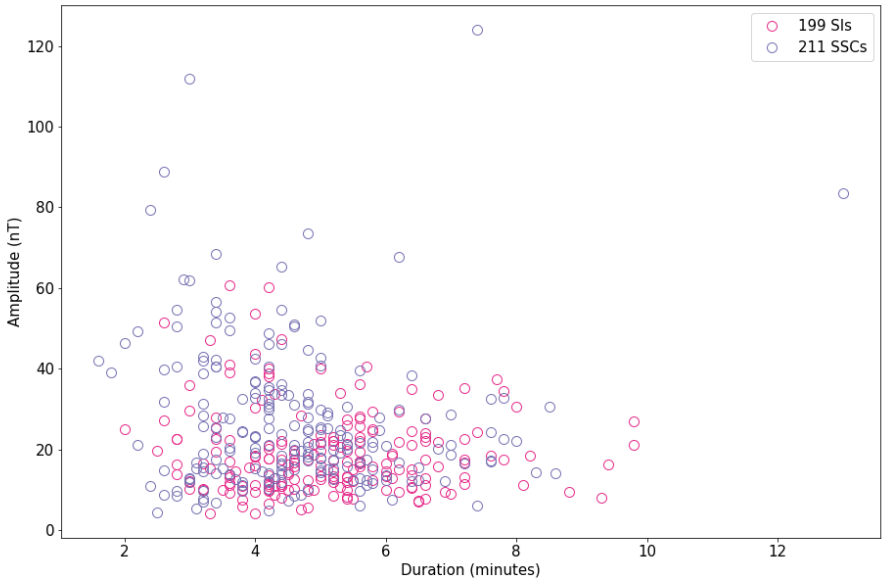

Figure 3. SC amplitude as a function of duration or 'rise time' for SIs in pink, and SSCs in purple from 1995-2017.

magnetosphere is not primed in any biased way preceding OE SCs. Although seemingly obvious, it is an important result that shows that the magnetosphere knows nothing of the pressure pulse until it arrives, and hence the SC is a result of pressure pulse compression.

The OE event list defines an SSC as any event where Dst or Kp reaches an empirical threshold within 48 hours. Firstly, this definition cannot be used in this study since events are only stratified by type from 2006 onwards. Secondly, given the dynamism of the Earth's space environment and the solar wind phenomena which can drive it, much can change within 48 hours, and so this definition may be too broad. Taylor et al. (1994); Taylor (1994) showed that for small SSCs, Dst (equivalent to SYM-H) reached -50 nT within 12 hours after onset of the characteristic rapid increase. For large SSCs, they showed that Dst reached -50 nT within 6 hours. Following on from this work, the OE SC events are further divided into SIs or SSCs based on a more relaxed empirical criterion than OE itself applies. An event is classified as an SSC if SYM-H reaches -40 nT within 12 hours of onset; this criterion was empirically adjusted based on the work by Taylor et al. (1994); Taylor (1994). Otherwise, an event is classified as an SI. Using this definition, 199 events are classified as SIs, and 211 are classified as SSCs. Of course, this definition is not infallible: within the 12 hours that follow onset, there could be, for example a change to strongly southward IMF, which in the end drives a geomagnetic storm, without which the event may have only been an SI. However, further classification of events based on potential driving phenomenon in the 12 hour window would be non-trivial, and is out of the scope of this paper.

Expanding on work by Araki et al. (2004) (whose study utilised 108 SCs), the amplitude of SC events is presented as a function of event duration or 'rise time' in Figure 3 for all events 1995-2017. Uniquely here, events are separated into SIs and SSCs using the revised definition described previously. Firstly considering the overall distribution,

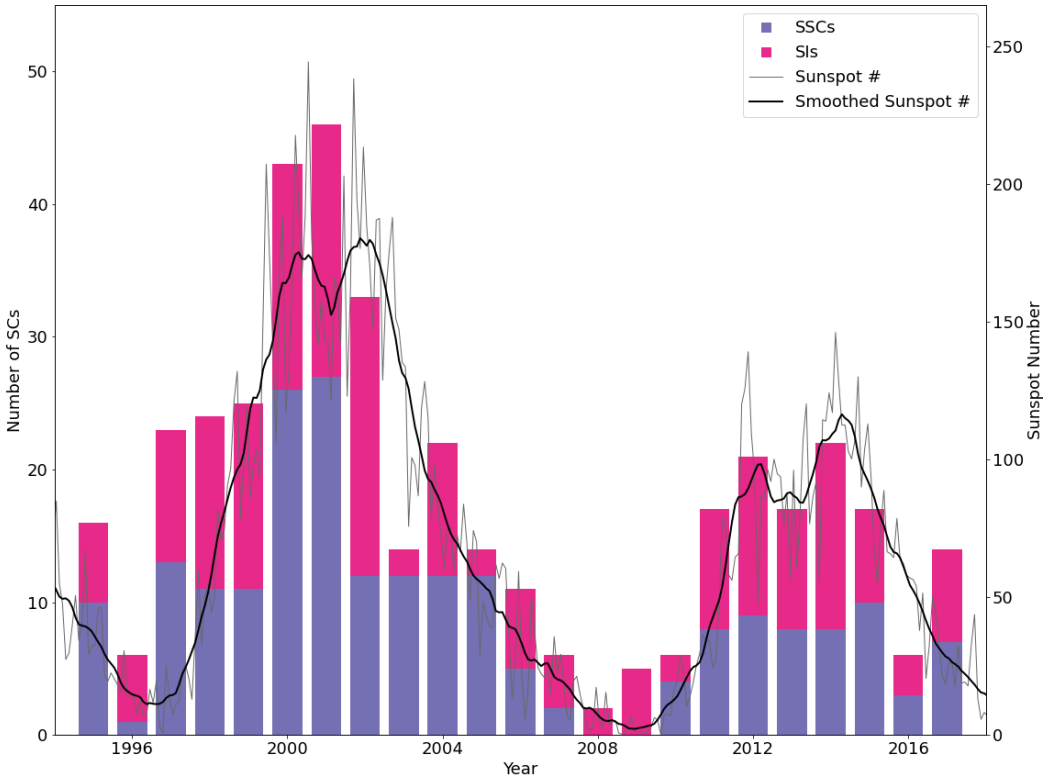

Figure 4. Number of SC events in each year from 1995 to 2017 inclusive. One bar per year; purple bar indicates SSCs, pink indicates SIs; purple and pink are stacked on top of each other. Monthly sunspot number shown in grey, smoothed monthly sunspot number shown in black.

there is a large cluster of events under around 20 nT amplitude (in keeping with the previously presented median of 19.04 nT) across a range of event durations, confirming results by Araki et al. (2004). Although most of the events fall within a similar amplitude-duration region, SSCs extend further in amplitude than SIs which plateau at around 60 nT amplitude. In duration, excluding one extreme SSC event, SIs tend to longer durations. Excluding two extreme SSCs, the distribution forms a similar decaying 'L' shape as that found by Araki et al. (2004), extending to higher amplitudes for SSCs.

3.1 Solar cycle dependence of SCs

The annual occurrence of SC events from 1995-2017 is presented in Figure 4; each bar is a stacked pair, pink indicates the number of SIs, and purple the number of SSCs. The combined height of both bars hence indicates the total number of SCs (which can be further subdivided into SIs and SSCs). The monthly sunspot number, a measure of solar cycle, is overplotted in grey, with a 13-month smoothed version in black; both were obtained from Sunspot Index and Long-term Solar Observations (SILSO) at the Royal Observatory of Belgium (2020). Broadly speaking, solar maximum denotes when the sunspot number peaks, and solar minimum is when the sunspot number is at its lowest point; this fluctuates on an 11 year cycle (e.g., Hathaway, 2015). There is a solar cycle dependency to the occurrence of both SIs and SSCs - more events are observed at solar maximum, and fewer at solar minimum. This alludes to the causes of SCs (investigating which is out of the scope of this study): Zuo et al. (2015) suggests that the majority of solar

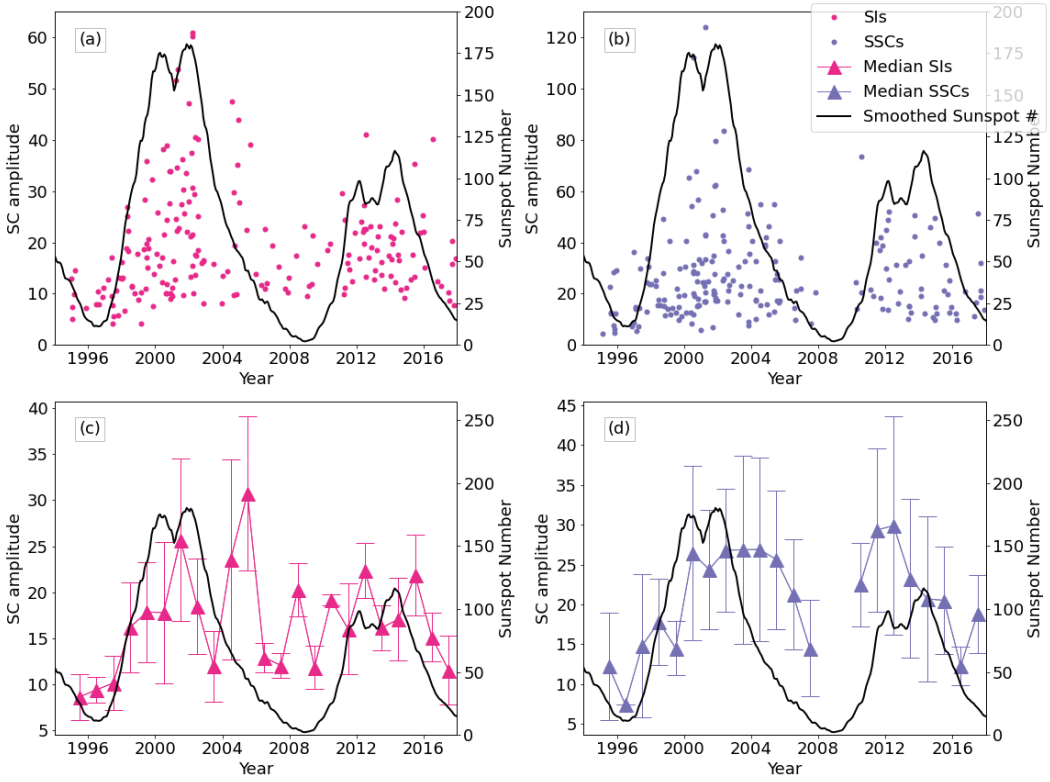

Figure 5. (a) SI event amplitude for events 1995-2017 (pink dots) with smoothed sunspot number overplotted in black. (b) SSC event amplitude for events 1995-2017 (purple dots) with smoothed sunspot number overplotted in black. (c) median SI amplitude for each year 1995-2017 (pink triangle, aligned halfway through the year as in 1995.5), with error bar showing median absolute deviation; smoothed sunspot number overplotted in black. (d) as for (c), but for SSCs (purple). Note that there are no SSCs in 2008/9, hence there is no median value for these years.

wind pressure pulses are generated by CMEs and CIRs, which have a solar cycle dependence, as discussed in the introduction.

Additionally, the solar cycle variation in SSCs shares some resemblance to the solar cycle dependence of major geomagnetic storms presented in Figure 23 of Gopalswamy (2022). In particular this is true for the second presented solar cycle: both the SSC variation of Figure 4 and Gopalswamy (2022)'s storm variation show a rather flat variation across the solar maximum. This resemblance relates to the shared properties of the two selected events, and adds weight to the definition of SSCs used in this paper, as it links back to geomagnetic storms selected via a different method.

Finally, the amplitude of SCs with respect to solar cycle is presented in Figure 5. The amplitude of all 199 SIs as a function of their onset time is presented in panel 5(a), with the smoothed sunspot number overplotted in black. Although there is a lot of variability in the data, the highest amplitude SIs occur during solar maximum, and fewer high amplitude SIs are observed at solar minimum. The median SI amplitude in each year from 1995-2017 is presented as pink triangles in panel 5(c); error bars show the median absolute deviation which is a robust measure of the variability in each median calculation (e.g., Sànchez-Cano et al., 2020; Lester et al., 2022). Although there is a great deal of variability from year to year, particularly with 2004-2005, there are some indi-

cators of increased SI magnitude around solar maximum, and decreased SI magnitude around solar minimum. This is particularly true in the ascending phase of the first presented solar cycle (1995 onwards), and the descending phase of the second presented solar cycle (2014 onwards).

The amplitude of all 211 SSCs as a function of their onset time is presented in panel 5(b). Similarly to SIs, the highest amplitude SSCs occur at solar maximum, and fewer of these high magnitude events are observed at solar minimum. It is important to note that the scale is different to panel 5(a) - for panel 5(b) the y-axis extends to over 120 nT, so displays some much higher magnitude events. The median SSC amplitude for each year from 1995-2017 is presented as purple triangles in Figure 5(d), with error bars representing the median absolute deviation, and the smoothed sunspot number overplotted in black. Despite some variability, in general greater SSC amplitude is observed at the peak of the solar cycle, and lower amplitude is observed at solar minimum. The median SSC amplitude curve seems slightly out of phase with the descending phase of the first presented solar cycle (2002 onwards). Overall, the median amplitude curve for SSCs seems to follow the solar cycle more clearly than for SIs.

The amplitude of SIs and SSCs reacts quite differently in the declining phase of the two presented solar cycles. In the first presented solar cycle (solar cycle 23), there is a bump in the declining phase in the magnitude of both SIs and SSCs: this links to observations of a large number of fast and/or wide CMEs (Gopalswamy et al., 2015), which caused shocks which in turn generated geomagnetic storms. For the next presented solar cycle (solar cycle 24), there are two peaks for SI magnitude (see Figure 5(c)), perhaps relating to the two sub-peaks in sunspot number. For SSCs, the smaller sunspot number sub-peak within cycle 24 results in larger amplitude SSCs, which may relate to more energetic CMEs.

4 Statistical differences between SIs and SSC

Using the stratification of SCs into SIs and SSCs described in the previous section, in this section the difference between both the driving pressure pulse and the preceding geomagnetic state for the two types of SC will be examined. Starting by comparing the differences in the driving event, in Figure 6 histograms of SC amplitude, duration and gradient. These are presented as in Figure 1 but with separate distributions for SIs (pink) and SSCs (purple). To quantify the differences between the distributions being compared, the Student's T-test is used. First devised by William S. Gosset (Student, 1908), the two sample T statistic quantifies the significance in the difference between two distributions. T is calculated from the ratio of the difference between the sample means, to the square root of the sum of the standard errors of the two samples (e.g., Vaughan, 2013). A larger value of T suggests greater difference between the two samples, and the sign of T indicates which sample mean is greater (here SSC values are compared with SI values, so positive T indicates that the SSC sample mean is greater).

To enhance interpretation, the p statistic is used to quantify the significance of the difference between the two samples. p is the probability that the differences between the two distributions occurred by chance, rather than some definite difference between the two samples. Generally $p<0.05$ is considered to indicate that the samples are different by means other than natural variability. More precisely, $p<0.05$ indicates that the null hypothesis can be rejected: the two samples are not from the same distribution. T and p values are presented in Tables 1 and 2**, along with sample means for SI and SSC distributions**.

In Figure 6(a), the distribution for SSCs is flatter than that for SIs, and extends to higher SC amplitudes. This is reflected in the amplitude medians **(which are recorded on the Figure)**: the median for SSCs is 21.9 nT, but only 16.9 nT for SIs. This sug-

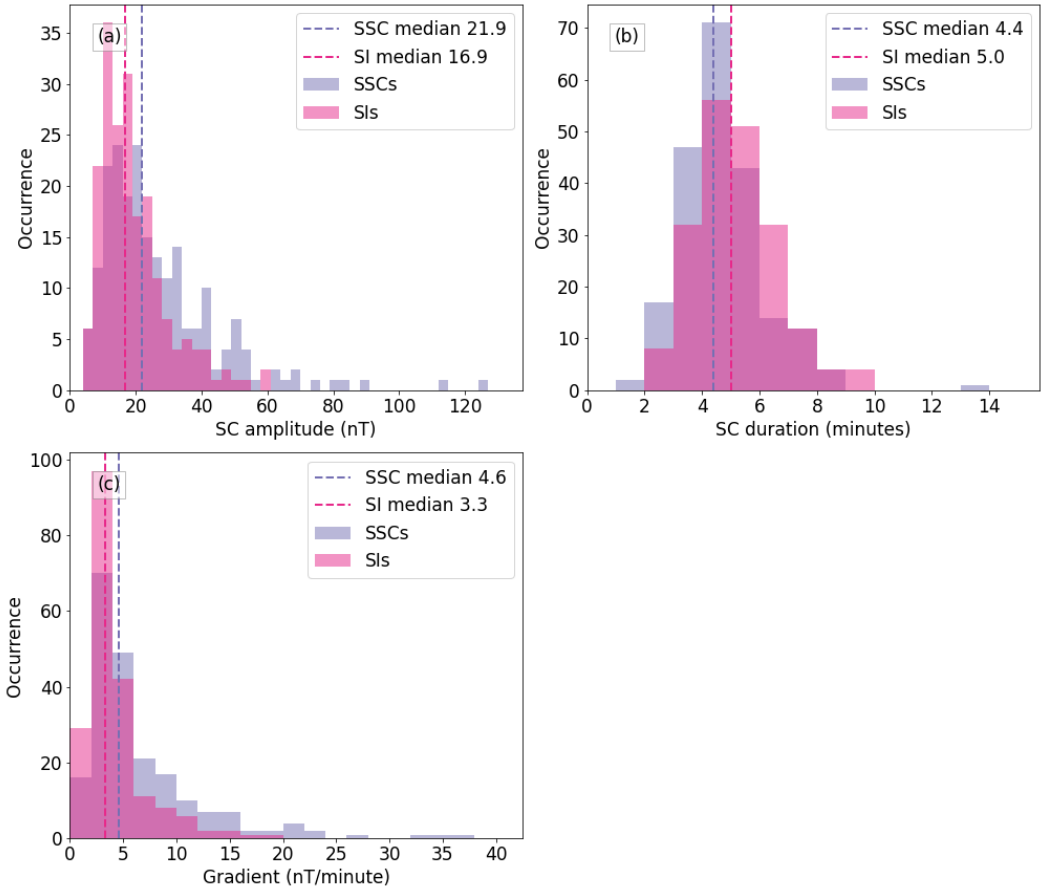

Figure 6. Histograms of SSC (a) event amplitude (b) event duration or 'rise time' (c) event rise gradient from the OE event list (410 events, 199 SIs and 211 SSCs). Pink histogram is for SIs, purple for SSCs; medians for distributions are indicated with dashed lines in corresponding colours.

Table 1. Table of statistics relating to the comparison between SSC and SI event characteristics presented in Figure 6. **Note that although the median is presented in Figure 6, the mean is presented here as it is used in calculation of the T statistic.** T statistic is from comparison of SSCs with SIs, hence positive indicates SSC sample mean is higher than the SI mean, while negative T indicates the SSC sample mean is lower.

Parameter	SI mean	SSC mean	T	p
SC amplitude	19.2	27.0	5.33	1.60×10^{-7}
SC duration	5.1	4.6	-3.41	7.24×10^{-4}
SC gradient	4.1	6.7	5.54	5.38×10^{-8}

gests that stronger events, or equivalently pressure pulses which compress the magnetosphere more, are more likely to drive a SSC than an SI; this may be since a larger amount of energy is communicated into the magnetosphere. The p value for this comparison is of the order 10^{-7} , far below the threshold value of 0.05, suggesting there is a difference between the SSC and SI distributions other than natural variability.

The distributions of event duration for SIs (pink) and SSCs (purple) are presented in Figure 6(b). The distribution for SIs and SSCs have similar shapes, but the distribution for SSCs is shifted towards shorter durations. This is demonstrated in the duration medians: the SSC distribution median is 4.4 minutes, whereas the SI distribution median is 5.0 minutes. This shows that shorter event durations are driving SSCs, which implies that more rapid magnetospheric compressions are more likely to generate an SSC than an SI. While this comparison has a negative T value, indicating that the SSC mean is smaller than the SI mean, the p value also falls far below the 0.05 threshold, indicating significant differences between the two distributions.

Finally, the distributions of event gradient (amplitude divided by duration) are presented in Figure 6(c), in pink for SIs and purple for SSCs. The distribution for SSCs spreads to higher gradients, which is reflected in the distribution medians - similar to the distributions for amplitude. The median gradient for SSCs is 4.6 nT minute^{-1}, almost 50% higher than the median gradient for SIs of 3.3 nT minute^{-1}. This suggests that larger, more rapid magnetospheric compressions are more likely to drive SSCs than SIs. Hence SSCs are driven by events in which greater energy is communicated into the system more rapidly than for SIs. This comparison is strengthened with a p value of the order of 10^{-8}, indicating significant differences between the two samples.

Next, the preceding geomagnetic state is assessed using geomagnetic indices and also by considering the average IMF and solar wind values which prime the magnetosphere before SC onset. The distributions of various parameters in the 30 minutes before SC onset are presented in Figure 7, parameterised by SIs (pink) and SSCs (purple). 30 mins was chosen as the preceding window, as a longer time period may include previous solar wind driving events, and a shorter time period may exclude geomagnetic activity which can vary on short timescales.

For IMF B_Z (panel 7(a)), both distributions are similar shapes, but the distribution is shifted towards negative values for SSCs, and positive for SIs. This suggests that a magnetosphere which has been primed by a southward IMF is more susceptible to SSCs at pressure pulse arrival. Conversely, the magnetosphere is more likely to be primed by northward IMF preceding SI onset. This comparison is made significant by a very low p value of the order of 10^{-68}. Since energy input into the magnetosphere is greatest under southward IMF, this suggests that a magnetosphere already primed with greater communication of solar wind energy into the magnetosphere is more likely to undergo an SSC.

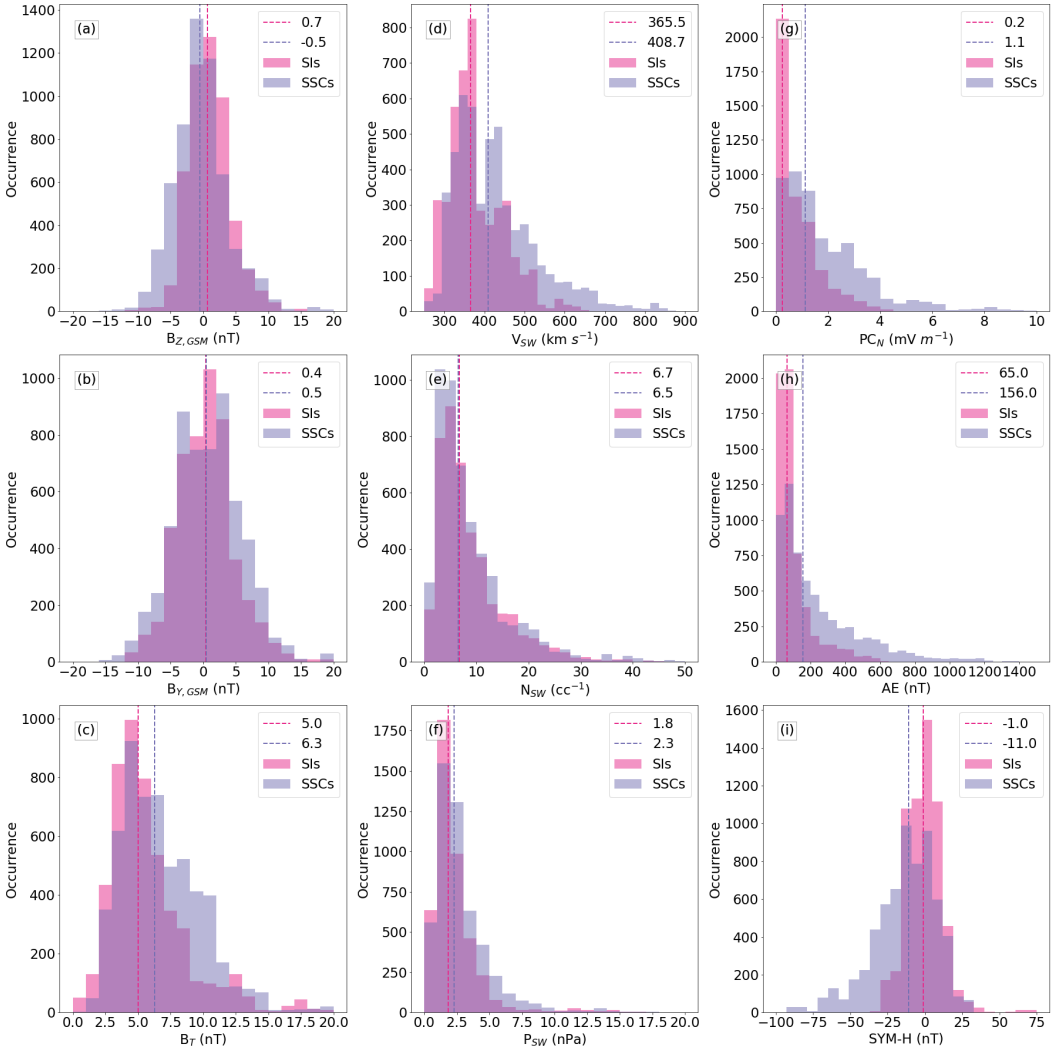

Figure 7. Histograms of (a) $B_{Z,GSM}$ (b) $B_{Y,GSM}$ (c) B_T (d) V_{SW} (e) N_{SW} (f) P_{SW} (g) PC_N (h) AE (i) SYM-H; pink shows distribution for SIs, purple for SSCs. Data taken from 30 minutes before SC onset. Median values for each distribution are indicated with dashed vertical lines in corresponding colours.

The distribution shapes and medians are similar for both SIs and SSCs for IMF B_Y, presented in Figure 7(b); although the p value meets the significance criterion, it is high compared with the other parameters. Still, there may be some difference between the two distributions. For the total IMF magnitude, B_T (panel 7(c)), the distribution is broader for SSCs and has a median over 20% higher than for SIs. This suggests that higher magnitude IMF is more likely to prime the magnetosphere for an SSC than an SI, this is confirmed by a very low p value of the order of 10^{-77}.

Distributions of the solar wind flow speed, V_{SW}, are presented in Figure 7(d). The distribution for SSCs is broader, and extends to higher values than for SIs. This is reflected in the medians for the distributions: for SIs the median is 365.5 km s^{-1}, slower than the median for SSCs of 408.7 km s^{-1}. Hence a faster solar wind speed is priming the magnetosphere preceding SSCs. This comparison is strengthened by one of the lowest calculated p values, of the order of 10^{-150}: this suggests there is a difference between

Table 2. Table of statistics relating to the comparison between SSC and SI event characteristics presented in Figure 7. **Note that although the median is presented in Figure 6, the mean is presented here as it is used in calculation of the T statistic.** T statistic is from comparison of SSCs with SIs, hence positive indicates SSC sample mean is higher than the SI mean, while negative T indicates the SSC sample mean is lower.

Parameter	SI mean	SSC mean	T	p
B_Z	1.0	-0.3	-17.62	1.46×10^{-68}
B_Y	0.4	0.7	2.70	6.88×10^{-3}
B_T	5.8	7.0	18.75	3.20×10^{-77}
V_{SW}	378.6	427.5	26.63	1.16×10^{-150}
N_{SW}	8.7	8.9	1.48	0.138
P_{SW}	2.4	2.9	10.53	9.18×10^{-26}
PC_N	0.4	1.7	7.72	1.30×10^{-14}
AE	103.2	247.9	41.24	0.00
SYM-H	-0.9	-14.1	-41.02	0.00

the two distributions other than natural variability. The distributions for solar wind density, N_{SW} (panel 7(e)), are similar, although the median is slightly higher for SIs than SSCs. This may suggest that the magnetosphere is primed by higher solar wind density for SIs, but the difference is only around 8%. However, the p value for N_{SW} is greater than 0.05, so the null hypothesis cannot be rejected. Therefore there is not a clear difference between the two distributions - so differences in solar wind density before SC onset are unlikely to be a controlling factor. For solar wind dynamic pressure, the distributions are again similar, although the distribution for SSCs is slightly broader; the p value meets the significance criterion. The median value for SSCs is about 17% higher, suggesting that the magnetosphere is compressed more before SSC onset than for SI onset, and this is dominated by a component of higher solar wind flow speed.

Finally, distributions of geomagnetic indices in the 30 minutes preceding SC onset are presented. Note that the p significance criterion is met for all three indices, with zero values for AE and SYM-H - see Table 2. These characterise internal magnetospheric activity before each SC. For the polar cap index, PC_N, presented in Figure 7(g) the distribution is broader, and has higher magnitude for SSCs than SIs. The median value for SIs is smaller than average values presented by Fogg et al. (2022), whereas the median value for SSCs is larger than average values. Hence there may be stronger than average polar ionospheric currents preceding SSCs, suggesting faster cross polar flow of magnetic flux. For the auroral electrojet index, AE, presented in Figure 7(h), the distribution is much broader for SSCs, with a median over twice as large as that for SIs. Therefore auroral activity is greater preceding SSCs, which may allude to other activity including substorms. Finally, the ring current index preceding SCs is presented in Figure 7(i). A much broader distribution is seen for SSCs, with a median ten times as negative. This may suggest that the magnetosphere is primed by storm activity before SSC onset, and less likely to be primed in this way before SI onset.

5 Superposed Epoch Analysis of SIs and SSCs

The average evolution of various solar wind and IMF parameters relative to SC onset will be described using a superposed epoch analysis. The onset of each event rounded down to the nearest minute is used as $t = 0$: the times are rounded down as this gives the integration window during which the event happens, rather than the next one if the time were rounded up. This is in keeping with the OMNI data which is minute resolu-

tion. The value of each parameter is extracted from 60 minutes before to 60 minutes after each event onset (note that the 60 minutes following onset will include the duration of the SC rise). These time series are arranged relative to onset time, and the median value across all events at each minute relative to onset time is extracted as the superposed epoch value. For each of these points, the median absolute deviation (η) is calculated as a robust measure of the amount of variability in each median calculation (e.g., Sànchez-Cano et al., 2020; Lester et al., 2022). These results are presented in Figure 8, with solid curves representing the median values and a shade showing $\pm 1\eta$.

The superposed epoch trace of IMF B_Z shows weakly negative B_Z before onset for SSCs, which increases in magnitude after onset. Conversely, the B_Z trace shows weakly positive B_Z before SI onset, but this also increases in magnitude after onset. This indicates moderate southward IMF following onset for SSCs, and moderate northward IMF for SIs: more energy is being communicated between the IMF and the magnetosphere under southward IMF, potentially helping to drive an SSC. The variability represented by $\pm 1\eta$ shows a broader parameter space following onset, which indeed is the case for most parameters and indicates the variability in the magnetospheric system after SC onset. For IMF B_Y, the median trace hovers around zero throughout the interval; this suggests there is no particular B_Y preference generating SIs or SSCs. For the total IMF magnitude, presented in panel 8(c), the magnitude is higher throughout for SSCs, and this difference increases after onset.

As suggested in the analysis from Figure 7, the solar wind flow speed (panel 8(d)) is higher throughout the interval for SSCs. However, for N_{SW} (panel 8(e)), the traces are very similar for both event types, relating to the non-significant differences between distributions presented in Figure 7 and Table 2. For solar wind dynamic pressure, P_{SW}, which is presented in panel 8(f), the trace for SSCs is slightly higher before onset, and this difference increases after onset. Hence the larger pressure for SSCs is dominated by an increase in flow speed, with little contribution from the density. This agrees with analysis from Figure 6, which suggested that SSCs are driven by events of higher magnitude i.e. a larger compression driven by a larger pressure increase.

Finally, the superposed epoch technique was applied to geomagnetic indices. The polar cap index, PC_N (panel 8(g)) shows a steady trace before onset with a short decrease at onset followed by an enhancement for both SC types. The values for SSCs are higher throughout, but the separation increases after onset. This may suggest initially a slowing of flux movement as the ionosphere reconfigures following SC onset, indicated by a drop on PC_N. This is followed by a rapid enhancement of antisunwards flux transport, indicated by an enhancement in PC_N. This may result as the incompressible ionosphere cannot instantaneously restructure: flows must slow down before they can change direction as the convection pattern restructures (this was observed by e.g., Fogg et al. (2023)).

For SIs, the AE index (panel 8(h)) is steady beforehand with a slight increase following onset; for SSCs, AE shows a sharp increase at onset, and steadily increases beyond that. This demonstrates greater activity in the auroral zone preceding and following SSCs than SIs, suggesting that SSCs follow a more active interval, and that this activity is enhanced by pressure pulse arrival. The ring current index, SYM-H (panel 8(i)) is steady for both event types before onset and rises sharply at onset. For SIs, SYM-H is around zero before onset, rises to positive values and remains steady after onset. For SSCs, SYM-H is at negative values before onset, rises sharply at onset (as a result of the increased magnetopause current causing an increase in the vertical component of the magnetic field in the equatorial plane (e.g., Araki, 1994; Fogg et al., 2023)) and begins to decay towards negative values almost immediately (indicating a move towards storm time). This suggests that SSCs are more likely to happen when the ring current is already energised, and hence is primed for a geomagnetic storm. This has some similarity to re-

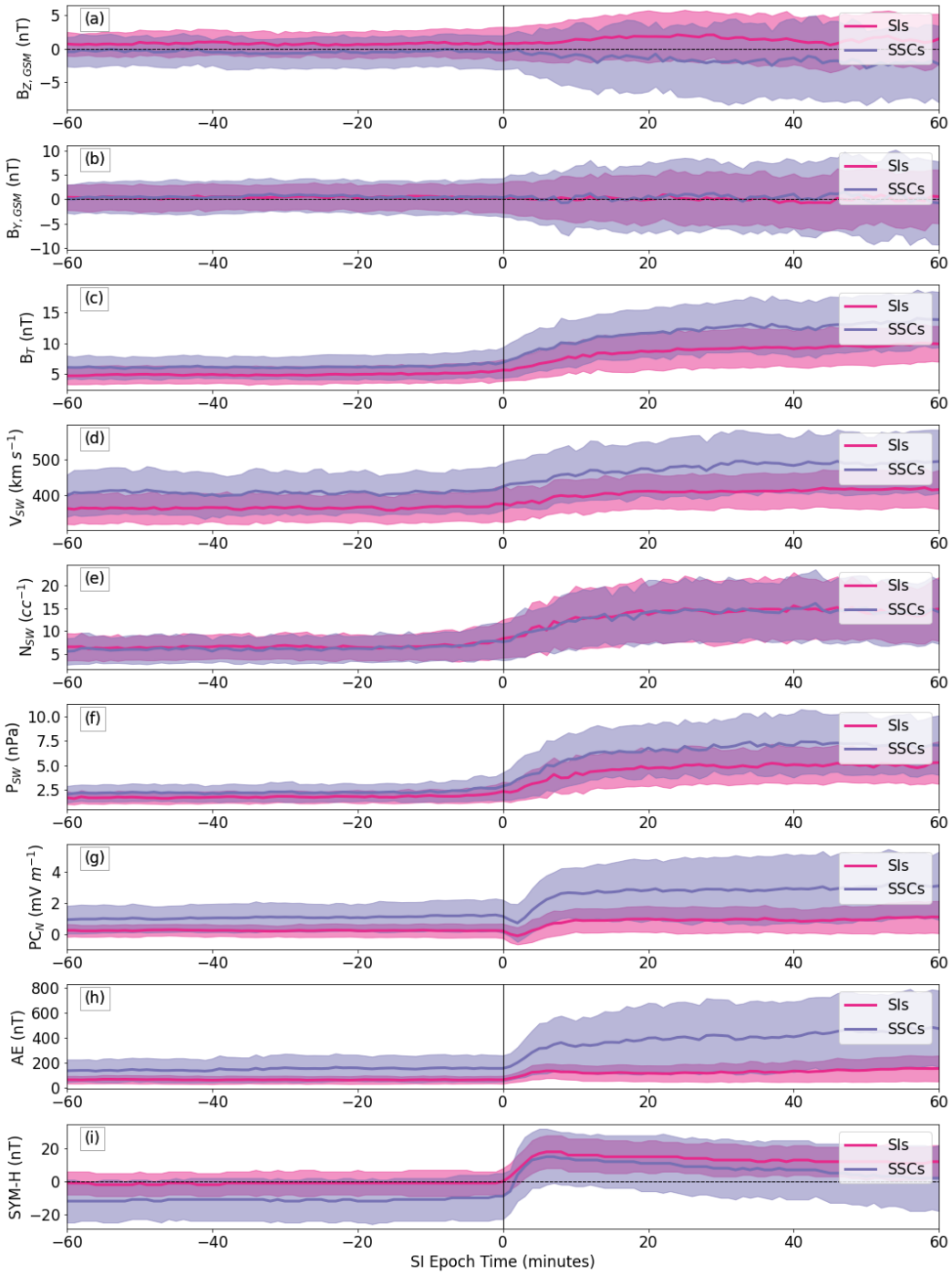

Figure 8. Superposed epoch analysis of (a) $B_{Z,GSM}$ (b) $B_{Y,GSM}$ (c) B_T (d) V_{SW} (e) N_{SW} (f) P_{SW} (g) PC_N (h) AE (i) SYM-H relative to SC onset. Solid line indicates the median value for each epoch time, shade shows $\pm 1\eta$. Traces in purple are for SSCs, in pink for SIs. A solid vertical line indicates onset time at $t = 0$; where appropriate, a dashed horizontal line indicates zero.

sults by Xie et al. (2008) who showed that preexisting ring currents can prolong storm duration.

To investigate the differences between the superposed epoch traces further, the difference between the two traces is presented in Figure 9 (SI trace - SSC trace). The difference between SIs and SSCs for B_Z presented in Figure 9(a) shows a difference of magnitude around 1 nT, rising to around 3 nT after onset. For B_Y, there is little difference before onset, but small fluctuating differences after onset, suggesting perhaps that there is a small B_Y component to the events driving SSCs which was hard to identify from Figure 8(b). Since a small amount of B_Y changes the reconnection sites this may suggest greater energy input from dayside reconnection (e.g., Grocott et al., 2003, 2004, 2008). For B_T, the difference plot presented in panel 9(c) shows that around SSC onset the IMF magnitude is greater, and that this difference increases after onset.

Panel 9(d) shows about 40 km s^{-1} faster solar wind speed before SSC onset, increasing gradually to 80 km s^{-1} after onset. For the solar wind density, there is little difference between the two, and there is a great deal of variability, however it could be argued that there is a slightly larger solar wind density leading up to SI onset, however the p value presented in Table 2 suggests the difference between distributions in this period is not significant. Panel 9(f) shows the difference between the two traces of solar wind dynamic pressure, demonstrating that solar wind pressure is slightly higher leading up to SSCs, and this increases to a difference of 2 nPa following onset (equal to the 2000-2004 average magnitude for P_{SW} presented by Fogg et al. (2022)).

The difference between the two traces of the polar cap index is presented in Figure 9(g), and shows an initially higher PC_N for SSCs, which rapidly increases to a difference of about 2 mV m^{-1} (a difference more than two times larger than the 2000-2004 median value reported by Fogg et al. (2022)). This suggests much faster cross polar convection of magnetic flux following SSC onset than SI onset, with some initial difference observed also. Similarly, for AE (panel 9(h)), values are about 100 nT larger preceding SSC onset, and this difference increases after onset to around 300 nT. This suggests greater auroral activity before SSC onset than SI onset, followed by even greater activity after onset for SSCs. Finally, the difference between SYM-H traces is presented in panel 9(i). Before onset, the SI trace is about 10 nT more positive than the SSC trace. This gap is almost closed at onset, as the SSC trace rises rapidly to positive values, almost meeting the SI trace. Then the SSC trace begins to decay to more negative values, and so the difference trace increases again, indicating more positive values for SIs. This shows that although the SSC trace begins in storm-like negative values, it increases rapidly to greater magnitude (as suggested by the amplitude distributions in Figure 6) than SIs, before beginning to decay back to storm-like negative values.

It is important to note that for some parameters, the differences between superposed epoch traces, presented in Figure 9, are small. This must caveat interpretation. However some conclusions can be made based on the evolution of the different parameters.

6 Discussion and Summary

SCs, like all space weather, can have a dramatic impact on the Earth's magnetosphere, and so understanding the differences between how pressure pulses drive the magnetosphere is of vital importance as society moves towards better prediction of space weather and mitigation of its effects. In this paper, the differences in situations where a solar wind pressure pulse drives a geomagnetic storm (an SSC) and otherwise (an SI) have been analysed. This will help to understand the effects of SCs on solar wind-magnetosphere-ionosphere coupling.

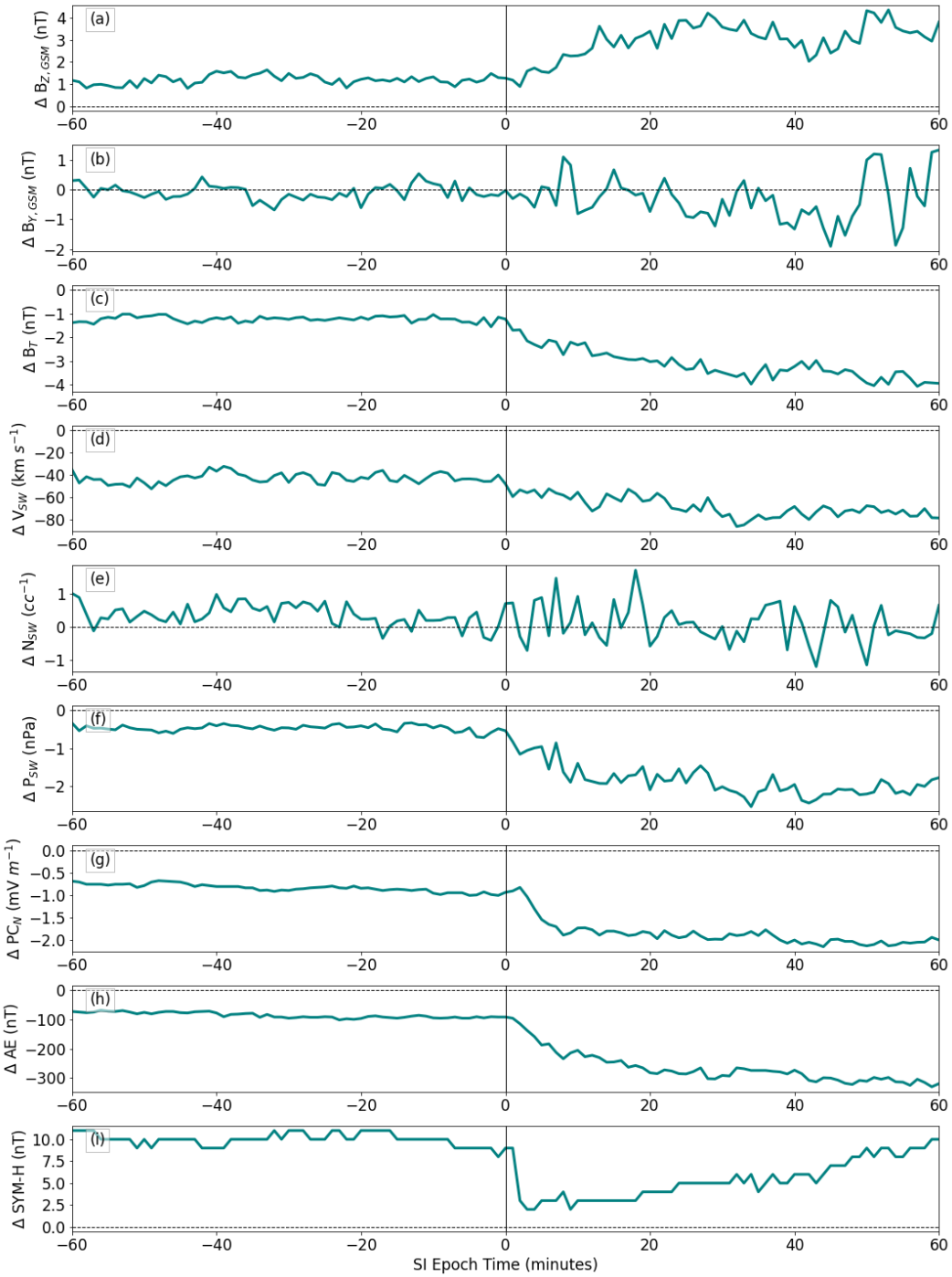

Figure 9. Difference between SI and SSC superposed epoch traces (SI trace - SSC trace) for (a) $B_{Z,GSM}$ (b) $B_{Y,GSM}$ (c) B_T (d) V_{SW} (e) N_{SW} (f) P_{SW} (g) PC_N (h) AE (i) SYM-H relative to SC onset. A solid vertical line indicates onset time at t=0; where appropriate, a dashed horizontal line indicates zero.

An interesting result from this study is that larger and/or faster magnetospheric compressions are more likely to result in SSCs. For example, a larger magnetospheric compression may communicate more energy (from a larger change in the solar wind) into the magnetosphere, which may lead to a build up of energy which then transforms into a geomagnetic storm. For more rapid compressions, the mechanism may be more subtle. In this case, energy is being driven more quickly into the magnetosphere; this may stimulate subtly different ULF wave activity which may be associated with storm dynamics. More rapid compressions could also lead to greater energy input into the magnetosphere overall than a slower compression of the same magnitude.

Additionally, it has been shown that in the 30 minutes preceding SC onset, the magnetosphere is primed by southward IMF and higher geomagnetic activity prior to SSCs, when compared with SIs. In the instance where southward IMF primes the magnetosphere, more energy is being communicated into the magnetosphere from the IMF and solar wind as a result of dayside magnetic reconnection, and so the magnetosphere is more susceptible to geomagnetic storms; indeed a period of sustained southward IMF is one of the preparatory factors in storm ignition (e.g., Walach & Grocott, 2019). In a similar sense, a higher solar wind speed and pressure preceding SSCs alludes to a magnetosphere that is already compressed, and hence more energised. Finally, when geomagnetic activity is higher in the 30 minutes preceding SC onset, the magnetosphere is already perturbed, and more susceptible to the triggering of a geomagnetic storm and hence an SC becoming an SSC.

Although there are apparent differences between the traces for SSCs and SIs in the superposed epoch analysis presented in Figure 8, there is some overlap in the median absolute deviation. For example, it is clear from the shade in panel 8(a) that although on average SSCs are preceded by southward IMF, some events are preceded by northward IMF. This leads to a question as to what the driving mechanism is between the pressure pulse compression itself, which links to the generation of a geomagnetic storm. Although southward IMF is the average, either B_Z sign is possible, so the pressure pulse itself must be driving the storm. Hence a question remains: what is the mechanism which links a magnetospheric compression to a geomagnetic storm? Are they related or are SSCs simply compressions which are coincidentally followed by a geomagnetic storm? The time-series of SYM-H presented in panel 8(i) supports the former: SYM-H begins to move towards storm values immediately after SC onset. A follow up study analysing the 12 hours that follow SC onset may help to shine light on this.

A summary of key results from the paper is given below:

1. There is a solar cycle dependence to the occurrence of both SIs and SSCs. More events are observed at solar maximum than solar minimum. The relationship between SSCs and sunspot number is more subtle, due to dependence on CMEs which can deviate from sunspot number.
2. More events of higher magnitude are observed at solar maximum than solar minimum for both SIs and SSCs. The average magnitude for SSCs follows the solar cycle more clearly.
3. SSCs are more likely to be driven by pressure pulses with higher magnitude and shorter duration than SIs.
4. The magnetosphere is primed by southward IMF (northward for SIs), larger IMF magnitude, faster solar wind speed and higher solar wind pressure for SSCs.
5. Geomagnetic indices suggest higher activity at polar, auroral, and equatorial latitudes preceding SSCs, when compared with SIs.
6. Following SC onset, SSCs see larger increases in IMF magnitude; for SSCs IMF B_Z becomes more negative, and for SIs B_Z becomes more positive. B_Y results are inconclusive.

7. Following SC onset, SSCs present larger increases in solar wind speed and pressure, there is some evidence SIs see larger solar wind density.
8. SSCs see larger magnitude geomagnetic indices before and after onset, and particularly see negative SYM-H values before onset.

In summary, it is both the contribution of the size of the pressure pulse event, and the preceding geomagnetic state that contributes to whether a pressure pulse triggers a geomagnetic storm. Additionally, the polarity of IMF B_Z before the onset of the SC contributes to the geoeffectiveness of the pressure pulse: southward IMF before pressure pulse arrival is more likely to drive an SSC. SSCs are more likely to be driven by SC events with higher magnitude, which has been shown to be proportional to the height of the pressure pulse itself (Siscoe et al., 1968; Russell et al., 1992; Takeuchi, Araki, et al., 2002); therefore SSCs are driven by larger solar wind pressure pulses than SIs. Similarly, SSCs are driven by more rapid pressure enhancements: it was found that SSCs have shorter rise times than SIs. Finally, SSCs are more likely to happen when the magnetosphere is primed by stronger solar wind and IMF conditions, and/or higher geomagnetic activity, perhaps even already in storm time.

Open Research Section

The sudden commencement event list used in this paper was compiled by Observatori de l'Ebre (Observatori de l'Ebre, 2020). Events are freely available from: `https://www.obsebre.es/en/rapid`. We gratefully acknowledge use of NASA/GSFC's Space Physics Data Facility's OMNIWeb (Papitashvili, N., 2023), (`https://omniweb.gsfc.nasa.gov/hw.html`) service, and OMNI data. The AE and SYM-H indices used in this paper were provided by the WDC for Geomagnetism, Kyoto (`http://wdc.kugi.kyoto-u.ac.jp/wdc/Sec3.html`) via OMNIWeb. PC(N) index was provided by World Data Center for Geomagnetism, Copenhagen via OMNIWeb. Sunspot data from the World Data Center SILSO (Sunspot Index and Long-term Solar Observations (SILSO) at the Royal Observatory of Belgium, 2020), Royal Observatory of Belgium, Brussels, and can be freely obtained from: `https://www.sidc.be/silso/datafiles`.

Acknowledgments

ARF's work was supported by Irish Research Council Government of Ireland Postdoctoral Fellowship GOIPD/2022/782. CMJ's work was supported by the Science Foundation Ireland Grant 18/FRL/6199. DMW's work at DIAS is funded by European Union's Horizon 2020 research and innovation programme under grant agreement No. 952439 and project number AO 2-1927/22/NL/GLC/ov as part of the ESA OSIP Nanosats for Spaceweather Campaign. ML acknowledges support from the UK Science and Technology Facilities Council grant ST/W00089X/1.

References

Araki, T. (1994). A physical model of the geomagnetic sudden commencement. *Geophysical Monograph*, *81*, 183–200. doi: 10.1029/GM081p0183

Araki, T., Fujitani, S., Emoto, M., Yumoto, K., Shiokawa, K., Ichinose, T., ... Liu, C. F. (1997). Anomalous sudden commencement on March 24, 1991. *Journal of Geophysical Research*, *102*(A7), 14075–14086. doi: 10.1029/96JA03637

Araki, T., Takeuchi, T., & Araki, Y. (2004). Rise time of geomagnetic sudden commencements - Statistical analysis of ground geomagnetic data. *Earth Planets Space*, *56*, 289–293. doi: 10.1186/BF03353411

Boudouridis, A., & Zesta, E. (2021). Automated Technique for the Detection of Step-Like Solar Wind Dynamic Pressure Changes: Application to the Response of the Transpolar Potential to Solar Wind Dynamic Pressure Fronts.

Journal of Geophysical Research: Space Physics, *126*(e2021JA029198). doi: 10.1029/2021JA029198

Boudouridis, A. E., Zesta, E., Lyons, L. R., Anderson, P. C., & Lummerzheim, D. (2003). Effect of solar wind pressure pulses on the size and strength of the auroral oval. *Journal of Geophysical Research*, *108*(A4). doi: 10.1029/2002JA009373

Burch, J. L. (1972). Preconditions for the triggering of polar magnetic substorms by storm sudden commencements. *Journal of Geophysical Research*, *77*(28), 5629–5632. doi: 10.1029/JA077i028p05629

Chi, P. J., Lee, D.-H., & Russell, C. T. (2006). Tamao travel time of sudden impulses and its relationship to ionospheric convection vortices. *Journal of Geophysical Research*, *111*(A08205). doi: 10.1029/2005JA011578

Chisham, G., Freeman, M. P., Coleman, I. J., Pinnock, M., Hairston, M. R., Lester, M., & Sofko, G. (2004). Measuring the dayside reconnection rate during an interval of due northward interplanetary magnetic field. *Annales Geophysicae*, *22*(12), 4243–4258. doi: 10.5194/angeo-22-4243-2004

Coco, I., Amata, E., Marcucci, M. F., Ambrosino, D., & Shepherd, S. G. (2011). Effects of Abrupt Variations of Solar Wind Dynamic Pressure on the High-Latitude Ionosphere. *International Journal of Geophysics*, *2011*. doi: 10.1155/2011/207514

Coco, I., Amata, E., Marcucci, M. F., Ambrosino, D., Villain, J. P., & Hanuise, C. (2008). The effects of an interplanetary shock on the high-latitude ionospheric convection during an IMF By-dominated period. *Annales Geophysicae*, *26*(9), 2937–2951. doi: 10.5194/angeo-26-2937-2008

Coco, I., Amata, E., Marcucci, M. F., De Laurentis, M., Villain, J. P., Hanuise, C., & Candidi, M. (2005). Effects on SuperDARN HF radar echoes on sudden impulses of solar wind dynamic pressure. *Annales Geophysicae*, *23*(5), 1771-1783. doi: 10.5194/angeo-23-1771-2005

Crooker, N. U. (1992). Reverse convection. *Journal of Geophysical Research: Space Physics*, *97*(A12), 19363–19372. doi: 10.1029/92JA01532

Crooker, N. U., Gosling, J. T., Bothmer, V., Forsyth, R. J., Gazis, P. R., Hewish, A., ... Wimmer-Schweingruber, R. F. (1999). CIR Morphology, Turbulence, Discontinuities, and Energetic Particles. , 179–220. doi: 10.1007/978-94-017-1179-1_12

Davis, T. N., & Sugiura, M. (1966). Auroral electrojet activity index AE and its universal time variations. *Journal of Geophysical Research*, *71*(3), 785–801. doi: 10.1029/JZ071i003p00785

Fogg, A. R. (2021). *SuperDARN Observations of High Latitude Electrodynamics in the Terrestrial Ionosphere* (Doctoral dissertation, University of Leicester School of Physics and Astronomy). doi: 10.25392/leicester.data.16621912.v1

Fogg, A. R., Jackman, C. M., Waters, J. E., Bonnin, X., Lamy, L., Cecconi, B., ... Louis, C. K. (2022). Wind/WAVES Observations of Auroral Kilometric Radiation: Automated Burst Detection and Terrestrial Solar Wind - Magnetosphere Coupling Effects. *Journal of Geophysical Research: Space Physics*, *127*(e2021JA030209). doi: 10.1029/2021JA030209

Fogg, A. R., Lester, M., Yeoman, T. K., Carter, J. A., Milan, S. E., Sangha, H. K., ... Vines, S. K. (2023). Multi-Instrument Observations of the Effects of a Solar Wind Pressure Pulse on the High Latitude Ionosphere: A Detailed Case Study of a Geomagnetic Sudden Impulse. *Journal of Geophysical Research: Space Physics*, *128*(e2022JA031136). doi: 10.1029/2022JA031136

Fujita, S. (2019). Response of the magnetosphere-ionosphere system to sudden changes in solar wind dynamic pressure. *Reviews of Modern Plasma Physics*, *3*(2). doi: 10.1007/s41614-019-0025-1

Fujita, S., Tanaka, T., Kikuchi, T., Fujimoto, K., Hosokawa, K., & Itonaga, M. (2003). A numerical simulation of the geomagnetic sudden commence-

ment: 1. Generation of the field-aligned current associated with the preliminary impulse. *Journal of Geophysical Research*, *108*(A12). doi: 10.1029/2002JA009407

Gillies, D. M., St. Maurice, J. P., McWilliams, K. A., & Milan, S. (2012). Global-scale observations of ionospheric convection variation in response to sudden increases in the solar wind pressure. *Journal of Geophysical Research: Space Physics*, *117*(A4). doi: 10.1029/2011JA017255

Gopalswamy, N. (2008). Solar connections of geoeffective magnetic structures. *Journal of Atmospheric and Solar-Terrestrial Physics*, *70*, 2078–2100. doi: 10.1016/j.jastp.2008.06.010

Gopalswamy, N. (2022). The sun and space weather. *Atmosphere*, *13*. doi: 10.3390/atmos13111781

Gopalswamy, N., Xie, H., Akiyama, S., Mäkelä, P., Yashiro, S., & Michalek, G. (2015). The peculiar behavious of halo coronal mass ejections in solar cycle 24. *The Astrophysical Journal Letters*, *804*(1). doi: 10.1088/2041-8205/804/1/L23

Gosling, J. T. (1996). Corotating and transient solar wind flows in three dimensions. *Annual Review of Astronomy and Astrophysics*, *34*(1), 35–73. doi: 10.1146/annurev.astro.34.1.35

Grocott, A., Badman, S. V., Cowley, S. W. H., Yeoman, T. K., & Cripps, P. J. (2004). The influence of IMF By on the nature of the nightside high-latitude ionospheric flow during intervals of positive IMF Bz. *Annales Geophysicae*, *22*(5), 1755–1764. doi: 10.5194/angeo-22-1755-2004

Grocott, A., Cowley, S. W. H., & Sigwarth, J. B. (2003). Ionospheric flow during extended intervals of northward but B_Y-dominated IMF. *Annales Geophysicae*, *21*(2), 509–538. doi: 10.5194/angeo-21-509-2003

Grocott, A., Milan, S. E., & Yeoman, T. K. (2008). Interplanetary magnetic field control of fast azimuthal flows in the nightside high-latitude ionosphere. *Geophysical Research Letters*, *35*(8). doi: 10.1029/2008GL033545

Hathaway, D. H. (2015). The Solar Cycle. *Living Reviews in Solar Physics*, *12*(4). doi: 10.1007/lrsp-2015-4

Hori, T., Shinbori, A., Fujita, S., & Nishitani, N. (2015). IMF-By dependence of transient ionospheric flow perturbation associated with sudden impulses: SuperDARN observations. *Earth, Planets and Space*, *67*(190). doi: 10.1186/s40623-015-0360-6

Imber, S. M., Milan, S. E., & Hubert, B. (2006). The auroral and ionospheric flow signatures of dual lobe reconnection. *Annales Geophysicae*, *24*(11), 3115–3129. doi: 10.5194/angeo-24-3115-2006

Iyemori, T. (1990). Storm-Time Magnetospheric Currents Inferred from Mid-Latitude Geomagnetic Field Variations. *Journal of Geomagnetism and Geoelectricity*, *42*(11), 1249–1265. doi: 10.5636/jgg.42.1249

Jackman, C. M., Achilleos, N., Bunce, E. J., Cowley, S. W. H., Dougherty, M. K., Jones, G. H., ... Smith, E. J. (2004). Interplanetary magnetic field at ∼9 AU during the declining phase of the solar cycle and its implications for Saturn's magnetospheric dynamics. *Journal of Geophysical Research: Space Physics*, *109*(A11203). doi: 10.1029/2004JA010614

King, J. H., & Papitashvili, N. E. (2005). Solar wind spatial scales in and comparisons of hourly Wind and ACE plasma and magnetic field data. *Journal of Geophysical Research: Space Physics*, *110*(A2). doi: 10.1029/2004JA010649

Kokubun, S. (1983). Characteristics of storm sudden commencement at geostationary orbit. *Journal of Geophysical Research*, *88*(A12), 10025–10033. doi: 10.1029/JA088iA12p10025

Lester, M., Sanchez-Cano, B., Potts, D., Lillis, R., Cartacci, M., Bernardini, F., ... Russell, A. (2022). The Impact of Energetic Particles on the Martian Ionosphere During a Full Solar Cycle of Radar Observations: Radar Blackouts.

Journal of Geophysical Research: Space Physics, *127*(e2021JA029535). doi: 10.1029/2021JA029535

Mendoza, B., Valdés-Galicia, J. F., Maravilla, D., & Lara, A. (2003). Spectral Analysis Results for Sudden Storm Commencements 1868-1996. *Advances in Space Research*, *31*(4). doi: 10.1016/S0273-1177(02)00804-9

Observatori de l'Ebre. (2020). *International service on rapid magnetic variations.* Retrieved from `http://www.obsebre.es/en/rapid` (Accessed on: 07-02-2020 [Dataset])

Ozturk, D. S., Zou, S., & Slavin, J. A. (2017). IMF By effects on ground magnetometer response to increased solar wind dynamic pressure derived from global MHD simulations. *Journal of Geophysical Research: Space Physics*, *122*, 5028–5042. doi: 10.1002/2017JA023903

Papitashvili, N. (2023). *Omniweb plus.* Retrieved from `https://omniweb.gsfc.nasa.gov/hw.html` ([Dataset])

Piersanti, M., & Villante, U. (2016). On the discrimination between magnetospheric and ionospheric contributions on the ground manifestation of sudden impulses. *Journal of Geophysical Research: Space Physics*, *121*(7). doi: 10.1002/2015JA021666

Russell, C. T., Ginskey, M., Petrinec, S., & Le, G. (1992). The Effect of Solar Wind Dynamic Pressure Changes on Low and Mid-Latitude Magnetic Records. *Geophysical Research Letters*, *19*(12). doi: 10.1029/92GL01161

Sànchez-Cano, B., Narvaez, C., Lester, M., Mendillo, M., Mayyasi, M., Holmstrom, M., ... Durward, S. (2020). Mars' ionopause: A matter of pressures. *Journal of Geophysical Research: Space Physics*, *125*(e2020JA028145). doi: 10.1029/2020JA028145

Shi, X., Lin, D., Wang, W., Baker, J. B. H., Weygand, J. M., Hartinger, M. D., ... Shepherd, S. G. (2022). Geospace Concussion: Global Reversal of Ionospheric Vertical Plasma Drift in Response to a Sudden Commencement. *Geophysical Research Letters*, *49*(e2022GL100014). doi: 10.1029/2022GL100014

Siscoe, G. L., Formisano, V., & Lazarus, A. J. (1968). Relation between Geomagnetic Sudden Impulses and Solar Wind Pressure Changes - An Experimental Investigation. *Journal of Geophysical Research: Space Physics*, *73*(15). doi: 10.1029/JA073i015p04869

Smith, A. W., Forsyth, C., Rae, J., Rodger, C. J., & Freeman, M. P. (2021). The impact of sudden commencements on ground magnetic field variability: Immediate and delayed consequences. *Space Weather*, *19*(e2021SW002764). doi: 10.1029/2021SW002764

Stauning, P. (2013). The Polar Cap index: A critical review of methods and a new approach. *Journal of Geophysical Research: Space Physics*, *118*, 5021–5038. doi: 10.1002/jgra.50462

Student. (1908). The probable error of a mean. *Biometrika*, *6*(1), 1–25. doi: 10.2307/2331554

Sunspot Index and Long-term Solar Observations (SILSO) at the Royal Observatory of Belgium. (2020). *Sunspot Index and Long-term Solar Observations (SILSO): Sunspot Number.* Retrieved from `http://www.sidc.be/silso/datafiles` (Accessed on: 23-04-2020 [Dataset])

Takeuchi, T., Araki, T., Viljanen, A., & Watermann, J. (2002). Geomagnetic negative sudden impulses: Interplanetary causes and polarization distribution. *Journal of Geophysical Research: Space Physics*, *107*(A7). doi: 10.1029/2001JA900152

Takeuchi, T., Russell, C. T., & Araki, T. (2002). Effect of the orientation of interplanetary shock on the geomagnetic sudden commencement. *Journal of Geophysical Research: Space Physics*, *107*(A12). doi: 10.1029/2002JA009597

Tamao, T. (1964). The structure of Three-dimensional Hydromagnetic Waves in a Uniform Cold Plasma. *Journal of Geomagnetism and Geoelectricity*, *16*(2), 89–

114. doi: 10.5636/jgg.16.89

Taylor, J. R. (1994). *The cause of magnetic disturbances in the earth's ionosphere* (Unpublished doctoral dissertation). University of Leicester Department of Physics and Astronomy.

Taylor, J. R., Lester, M., & Yeoman, T. K. (1994). A superposed epoch analysis of geomagnetic storms. *Annales Geophysicae*, *12*(7), 612–624. doi: 10.1007/s00585-994-0612-4

Troshichev, O. A., & Andrezen, V. G. (1985). The relationship between interplanetary quantities and magnetic activity in the southern polar cap. *Planetary Space Science*, *33*(4), 415–419. doi: 10.1016/0032-0633(85)90086-8

Troshichev, O. A., Dmitrieva, N. P., & Kuznetsov, B. M. (1979). Polar cap magnetic activity as a signature of substorm development. *Planetary and Space Science*, *27*(3), 217–221. doi: 10.1016/0032-0633(79)90063-1

Vaughan, S. (2013). *Scientific Inference: Learning from data*. Cambridge University Press.

Veenadhari, B., Selvakumaran, R., Singh, R., Maurya, A. K., Gopalswamy, N., Kumar, S., & Kikuchi, T. (2012). Coronal mass ejection-driven shocks and the associated sudden commencements/sudden impulses. *Journal of Geophysical Research: Space Physics*, *117*(A4). doi: 10.1029/2011JA017216

Walach, M.-T., & Grocott, A. (2019). SuperDARN Observations During Geomagnetic Storms, Geomagnetically Active Times and Enhanced Solar Wind Driving. *Journal of Geophysical Research: Space Physics*, *124*(7), 5828–5847. doi: 10.1029/2019JA026816

Weimer, D. R., & King, J. H. (2008). Improved calculations of interplanetary magnetic field phase front angles and propagation time delays. *Journal of Geophysical Research: Space Physics*, *113*(A1). doi: 10.1029/2007JA012452

Weimer, D. R., Ober, D. M., Maynard, N. C., Burke, W. J., Collier, M. R., McComas, D. J., ... Smith, C. W. (2002). Variable time delays in the propagation of the interplanetary magnetic field. *Journal of Geophysical Research: Space Physics*, *107*(A8). doi: 10.1029/2001JA009102

Weimer, D. R., Ober, D. M., Maynard, N. C., Collier, M. R., McComas, D. J., Ness, N. F., ... Watermann, J. (2003). Predicting interplanetary magnetic field (IMF) propagation delay times using the minimum variance technique. *Journal of Geophysical Research: Space Physics*, *108*(A1). doi: 10.1029/2002JA009405

World Data Center for Geomagnetism Kyoto, Nose, M., Iyemori, T., Sugiura, M., & Kamei, T. (2015). *Geomagnetic AE index.* Retrieved from `https://doi.org/10.17593/15031-54800`

Xie, H., Gopalswamy, N., St. Cyr, O. C., & Yashiro, S. (2008). Effects of solar wind dynamic pressure and preconditioning on large geomagnetic storms. *Geophysical Researh Letters*, *35*(L06S08). doi: 10.1029/2007GL032298

Zuo, P., Feng, X., Xie, Y., Wang, Y., & Xu, X. (2015). Strong solar wind dynamic pressure pulses: Interplanetary sources and their impacts on geosynchronous magnetic fields. *The Astrophysical Journal*, *812*(2). doi: 10.1088/0004-637X/812/2/152